BULLETIN OF THE POLISH ACADEMY OF SCIENCES
TECHNICAL SCIENCES, Vol. 71(1), 2023, Article number: e144581
DOI: 10.24425/bpasts.2023.144581

Damage localization in truss girders by an application of the discrete wavelet transform

Anna KNITTER-PIĄTKOWSKA*, Olga KAWA, and Michał Jan GUMINIAK

Poznan University of Technology, Institute of Structural Analysis, Poland

Abstract. The paper demonstrates the potential of wavelet transform in a discrete form for structural damage localization. The efficiency of the method is tested through a series of numerical examples, where the real flat truss girder is simulated by a parameterized finite element model. The welded joints are introduced into the girder and classic code loads are applied. The static vertical deflections and rotation angles of steel truss structure are taken into consideration, structural response signals are computed at discrete points uniformly distributed along the upper or lower chord. Signal decomposition is performed according to the Mallat pyramid algorithm. The performed analyses proved that the application of DWT to decompose structural response signals is very effective in determining the location of the defect. Evident disturbances of the transformed signals, including high peaks, are expected as an indicator of the defect existence in the structure. The authors succeeded for the first time in the detection of breaking the weld in the truss node as well as proved that the defect can be located in the diagonals.

Key words: truss structures; damage localization; finite element method; discrete wavelet transform.

1. INTRODUCTION

Damage can be defined as a change in the material such as void, inclusion, crack, or delamination. When it occurs in a structural element, it can seriously interfere with its load-bearing capacity. Early detection, localization and estimation of structural damage is currently one of the most important engineering problems that has attracted much attention over the last years. Nondestructive testing is a relatively young and developing field of science. There are different nondestructive techniques which facilitate the identification of the defective part of a structure; most of them are based on the analysis of the structural response signals. Various approaches and many advanced techniques have been developed, e.g., radiography [1], ultrasonic [2, 3], acoustic emission [4], magnetic field [5] and eddy current [6] methods. Infrared and thermal testing [7, 8] or making use of an RGB-D camera [9] also proved to be an effective method in structural health monitoring. A great potential is assigned to soft methods, mainly evolutionary algorithms [10, 11] and artificial neural networks [12, 13].

Different types of structural response, namely eigenfrequencies/eigenmodes, displacements, angles of rotation, velocities, and/or accelerations can be useful to assess the reliability of the structure. Nevertheless, it happens that such a response is rather insensitive to damage localized in a small area, thus the localization of the defect is not easy to identify. The method used to extract the desired detailed information from numerous data representing the global response of a defective structure is called wavelet transform (WT). In this paper, it is applied in its discrete form (DWT). An indicator of the damage presence and location in this type of analysis is the strong disturbance of the transformed signal. There are many wavelet functions, e.g., Haar wavelet, Symlet, Coiflet, Meyer, Gaussian, Mexican hat, or Morlet, and new ones are constantly developed. Previous studies of the authors [14–16] proved that, in the class of considered problem, the most effective appeared to be the Daubechies wavelet [17]. The comparison between the efficiency of Haar, Daubechies and Coiflet wavelet in damage detection was discussed in [18]. Wavelet functions proved to be highly useful in many applications as well, including their implementation in the homogenization theory [19]. However, for the characterization of damage details such as type, intensity and size, in the locally defective elements of the structure, a combination of WT with additional tools such as inverse analysis [20, 21] or artificial neural networks [22] is necessary.

2. THEORETICAL FOUNDATION OF DWT

2.1. Mathematical background

Let the function $\psi(t)$, called the wavelet function (mother function), be continuous and belong to the field of $L^2(\boldsymbol{R})$. The function $\psi(t)$ satisfies the condition of admissibility [23]. The mother function may be real- or complex-valued. The real-valued wavelets will be applied in the present cases. For signal decomposition, the set of wavelets named the wavelet family is needed. This set of these functions is obtained by translating and scaling the function ψ:

$$\psi_{a,b} = \frac{1}{\sqrt{|a|}} \cdot \psi\left(\frac{t-b}{a}\right), \tag{1}$$

where t is a time or space coordinate, a and b are the scale and translation parameters, respectively. The parameters a and

*e-mail: anna.knitter-piatkowska@put.poznan.pl

Manuscript submitted 2022-06-30, revised 2022-12-07, initially accepted for publication 2022-12-10, published in February 2023.

b take real values ($a, b \in (\boldsymbol{R})$) and, additionally, $a \neq 0$. The element $|a|^{-1/2}$ expresses the scale factor which ensures the constant wavelet energy regardless of the scale, i.e., $\|\psi_{a,b}\| = \|\psi\| = 1$. In the current analysis, discrete wavelet transform (DWT) takes place as the main factor. The wavelet family can be derived by the substitution $a = 1/2^j$ and $b = k/2^j$ in equation (1). This leads to the relation:

$$\psi_{j,k}(t) = 2^{(j/2)} \cdot \psi\left(2^j \cdot t - k\right), \tag{2}$$

in which k and j are scale and translation parameters, respectively.

The discrete wavelet transformation (DWT) of the signal $f(t)$ is expressed by the following equation:

$$Wf(j,k) = 2^{j/2} \cdot \int_{-\infty}^{\infty} f(t) \cdot \psi\left(2^j \cdot t - k\right) \cdot \mathrm{d}t = \left\langle f(t), \psi_{j,k} \right\rangle. \tag{3}$$

The scalar product of the response function $f(t)$ and the wavelet function allows us to find the set of wavelet coefficients $d_{j,k} = \left\langle f(t), \psi_{j,k} \right\rangle$. This enables the discrete signal to be represented in the form of the combination of linear wavelet functions $\psi_{j,k}$ with wavelet coefficients $d_{j,k}$ which can be written as:

$$f(t) = \sum_{j=0}^{J-1} \sum_{k} d_{j,k} \cdot \psi_{j,k}(t) \tag{4}$$

for the number of discrete input data equal to 2^J.

The multi-resolution analysis is carried out with the use of the scaling wavelet function named the father function $\phi_{j,k}(t)$:

$$\phi_{j,k}(t) = 2^{j/2} \cdot \phi\left(2^j \cdot t - k\right). \tag{5}$$

The scaling function $\phi_{j,k}(t)$ limits the unit area and has the unit energy. This condition is described by the relation:

$$\int_{-\infty}^{\infty} \phi(t) \cdot \mathrm{d}t = 1. \tag{6}$$

This function fulfills the orthogonality and the translation conditions that can be expressed mathematically:

$$\left\langle \phi(t), \phi(t) \right\rangle = \int_{-\infty}^{\infty} |\phi(t)|^2 \cdot \mathrm{d}t = 1 \tag{7}$$

and

$$\left\langle \phi(t), \phi(t-n) \right\rangle = 0 \tag{8}$$

for $n \neq 0$.

The input signal as a function $f(t)$ is developed in series while using the basic (called mother) function $\psi(t)$ and the scaling (called father) function $\phi(t)$

$$f(t) = \sum_{k=-\infty}^{\infty} a_{j,k} \cdot \phi_{j,k}(t) + \sum_{k=-\infty}^{\infty} \sum_{j=0}^{\infty} d_{j,k} \cdot \psi_{j,k}(t), \tag{9}$$

where $a_{j,k}$ are the coefficients of the scaling wavelet determined as:

$$a_{j,k} = \left\langle f(t), \phi_{j,k} \right\rangle. \tag{10}$$

For 1-D DWT analysis, which will be applied in the current investigation, the decomposition of the discrete signal is carried out according to the Mallat pyramid algorithm [23]:

$$f_J = S_J + D_J + \ldots + D_n + \ldots + D_1 \tag{11}$$

for $n = J - j$, wherein each of the components in the signal representation is coupled with a specific range of the frequency and has the information at the scale level ($j = 1, \ldots, J$). Figure 1 illustrates the Mallat pyramid algorithm.

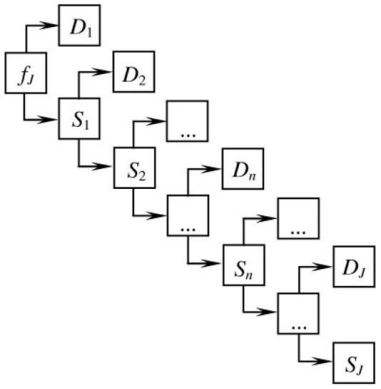

Fig. 1. The Mallat pyramid algorithm applied to the 1-D analysis

The parameter J describes the level of a multi-resolution analysis (MRA), S_J expresses the smooth signal representation, D_n and S_n are the details and rough parts of the transformed signal, respectively. Finally, D_1 corresponds to the most detailed representation of the transformed signal. The function f_J must be represented by $N = 2^J$ discrete values to fulfill the dyadic requirements of DWT.

Basic and scaling functions of Daubechies 4 wavelets which will be applied in the current investigations are presented in Fig. 2.

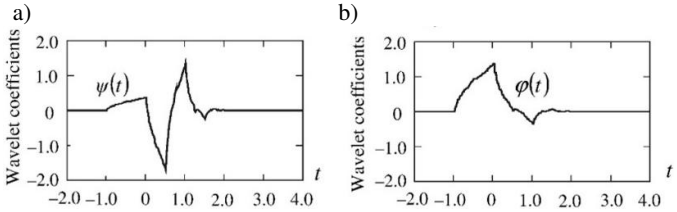

Fig. 2. Daubechies 4 wavelet function: a) basic (mother) and b) scaling function (father)

3. THE FINITE ELEMENT ANALYSIS

The statics of a system of flat truss girders is described and solved in terms of the finite element method, with the well-known governing equation for the considered structure:

$$\mathbf{K} \cdot \mathbf{q} = \mathbf{P}, \tag{12}$$

where **K**, **q** and **P** express the stiffness matrix, the displacement vector and the right-hand-side vector of the whole structure respectively, coupled with the appropriate boundary conditions introduced.

The two-node spatial bar finite element shown in Fig. 3 is applied in the numerical investigation of the structural response signal. It is also assumed that the cross-section deplanation is not blocked which is a simplifying assumption in the present FEM analysis.

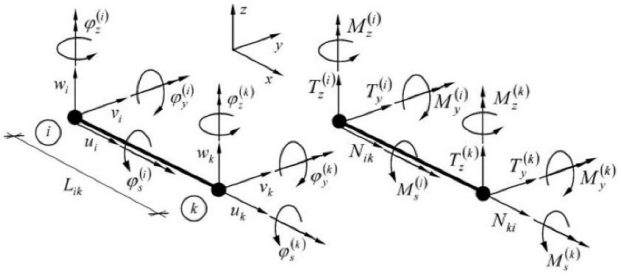

Fig. 3. Two-node spatial bar finite element

4. NUMERICAL EXAMPLES

This paper aims to localize the weakened parts of the structure under the condition that damage (e.g., deterioration) occurs in the examined element. The numerical models of the truss girders are tested to confirm the effectiveness of the presented damage detection method. In this section, six cases are discussed.

The flat truss girders subjected to classic code loads were analyzed. In the literature, examples of similar structure analyses can be found [24,25]. The ideal truss structure has the members connected at their ends by frictionless pin joints. In the study, the real flat truss girder is simulated, therefore, the welded joints are taken into consideration. The structural static response signal was obtained from the ROBOT Structural Analysis computational program while using the finite element method (FEM) and by applying 3D two-node finite elements (Fig. 3).

The following structural response signals were taken into consideration: the deflection line, angles of rotation of the lower and upper chord of the examined girder and, in addition, horizontal displacements of the selected diagonal. In order to simulate the work of a real structural element, the most unfavorable load combinations were selected for analysis in accordance with the applied engineering practice.

The response signal was transformed while using DWT procedures. The set of Daubechies 4, 6 and 8 families of wavelet functions were applied to the preliminary analysis. As an indicator of the damage presence in the structural element, the disturbances of the transformed signal are expected. Before analyzing the structure, both the ultimate limit state (ULS) and serviceability limit state (SLS) were verified. The introduced impairments were chosen in order not to exceed either the ULS or the SLS.

4.1. Example 1. Deterioration of the lower chord

In this example, the system of flat truss girders shown in Fig. 4 is analyzed. The span and the height of the examined truss girder are 24.0 m and 1.65 m, respectively. The upper and lower chords are made of steel hot-rolled profiles, i.e., HEB 300 and HEB 200. The diagonals are made of a thin-walled square hollow section of $120 \times 120 \times 6$ mm.

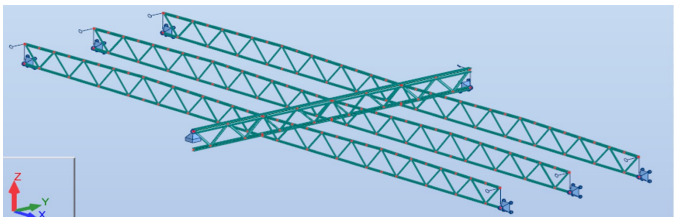

Fig. 4. Analyzed system of seven flat truss girders

The lower girder chord is divided into 160 finite elements and it is weakened by the replacement of the cross-section of one finite element with HEB 180 profile, thus there was a change in the geometrical characteristics simulating the deterioration. The basic dimensions and material properties of steel structural elements are given in Table 1.

Table 1
Element and material properties

Element	Profile	Material	Young's modulus
Upper chord	HEB 300	S355	$210 \cdot 10^6$ [kPa]
Lower chord	HEB 200	S355	$210 \cdot 10^6$ [kPa]
Chords-w	HEB 180	S355	$210 \cdot 10^6$ [kPa]
Diagonals	RK $120 \times 120 \times 6$	S355	$210 \cdot 10^6$ [kPa]
Diagonals-w	RK $90 \times 90 \times 5$	S355	$210 \cdot 10^6$ [kPa]

"Chords-w", "Diagonals-w" placed in the Table 1 denote the profiles assigned to the weakened cross-sections.

The sets of permanent and varying loads acting on the entire structure are given in Tables 2 and 3. The self-weight of the structure is embedded into a computational program.

Table 2
Permanent loads

Permanent (self-weight)	Value	Width	Characteristic value
$\gamma_f = 1.35$	[kN/m^2]	[m]	[kN/m]
Roof	0.32	6.0	1.92

Table 3
Varying loads

Varying loads	Value	Width	Characteristic value
$\gamma_f = 1.5$	[kN/m^2]	[m]	[kN/m]
Hangers, installations	0.15	6.0	0.9
Snow	0.72	6.0	4.32
Wind, zone H – suction	– 0.51	6.0	3.06
Wind, zone I – pressure	0.15	6.0	0.9

The deterioration of the lower chord bearing capacity was considered. The initial location of the weakened cross-section is shown in Fig. 5 in the relation to the entire single girder, whereas Fig. 6 shows the weakened cross-section in the relation to finite element division. The detail of the lower chord cross-section impairment is presented in Fig. 7. The weakened part of the lower chord is marked by a red circle in Fig. 5.

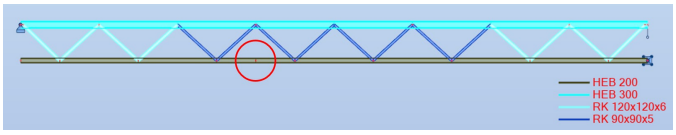

Fig. 5. Initial location of the weakened cross-section in the relation to the considered part of the whole structure

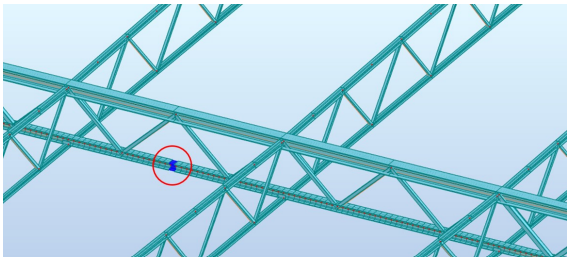

Fig. 6. Initial location of the weakened cross-section in the relation to the finite element division

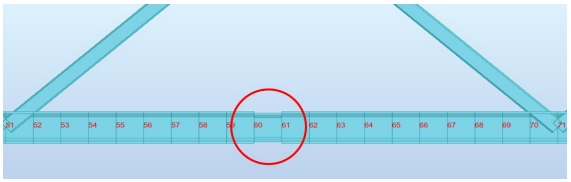

Fig. 7. Reduction of the cross-sectional stiffness in the relation to the undamaged part of the structure and finite element division

The lower chord deflection line, registered at discrete points, as the structure response signal was subjected to DWT analysis. The damage position is precisely indicated while employing the DWT procedure and Daubechies 4, 6 and 8 sets of wavelet functions, which is shown in Figs. 8–10.

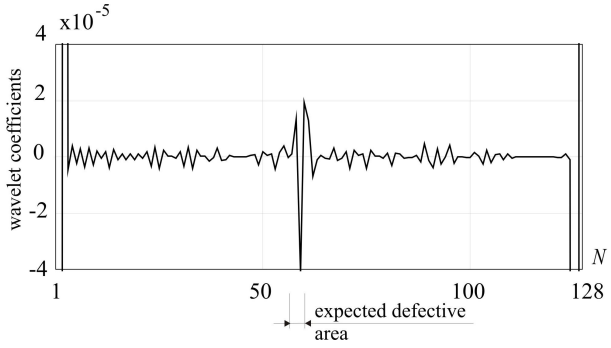

Fig. 8. 1-D DWT of angles of rotation for Daubechies 4 (detail 1) and $N = 128$ number of measurements

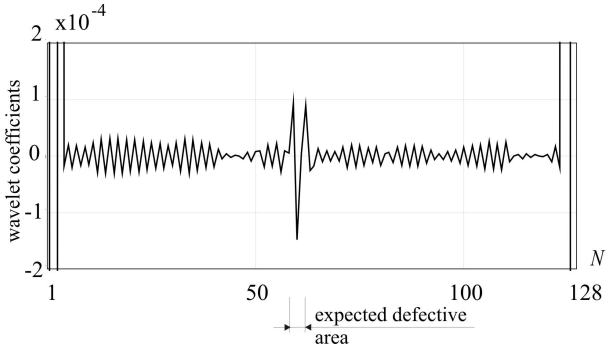

Fig. 9. 1-D DWT of vertical displacements for Daubechies 6 (detail 1) and $N = 128$ number of measurements

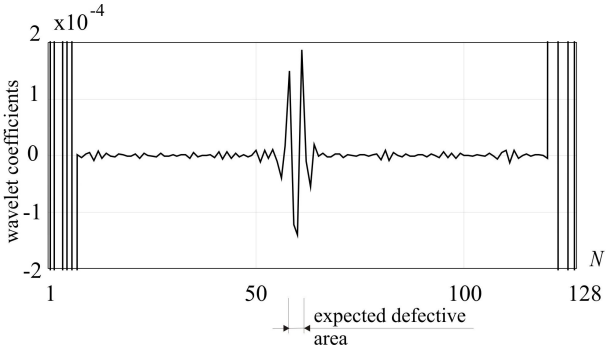

Fig. 10. 1-D DWT of vertical displacements for Daubechies 8 (detail 1) and $N = 128$ number of measurements

4.2. Example 2. Deterioration of the upper chord

In this example, the truss girder shown in Fig. 11 is analyzed.

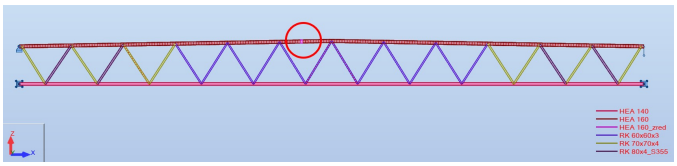

Fig. 11. Initial location of the weakened cross-section in the relation to the considered part of the whole structure

The height of the truss is 1.75 m, and the span is 24 m. The profiles and material properties of steel structural elements are listed in Table 4. The Young's modulus for all profiles is

Table 4
Element and material properties

Element	Profile	Material	I_y
Upper chord	HEA 160	S355	1670 [cm^4]
Upper chord – w	HEA 160	S355	1336 [cm^4]
Lower chord	HEA 140	S235	1033 [cm^4]
Diagonals	RK 80 × 80 × 4	S355	111 [cm^4]
	RK 70 × 70 × 4 RK 60 × 60 × 3	S235	74.7 [cm^4] 36.2 [cm^4]

$210 \cdot 10^6$ [kPa]. The permanent and varying loads are presented in Tables 5 and 6. The failure of the upper chord was introduced as a reduction of the cross-section stiffness. Moment of inertia I_y was reduced by 20 percent. The initial location of the weakened cross-section is shown in Fig. 11 in the relation to the entire single girder, whereas Fig. 12 shows the weakened cross-section in the relation to finite element division.

Table 5
Permanent loads

Permanent (self-weight)	Value	Width	Characteristic value
$\gamma_f = 1.35$	[kN/m^2]	[m]	[kN/m]
Roof	0.3	6.0	1.8

Table 6
Varying loads

Varying loads	Value	Width	Characteristic value
$\gamma_f = 1.5$	[kN/m^2]	[m]	[kN/m]
Hangers, installations	0.35	6.0	2.1
Snow	0.72	6.0	4.32
Wind, zone H – suction	– 0.51	6.0	3.06
Wind, zone I – pressure	0.15	6.0	0.9

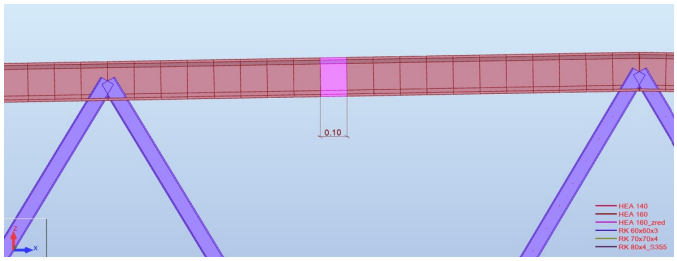

Fig. 12. Reduction of the cross-sectional stiffness in the relation to the undamaged part of the structure and finite element division

In the case of the discrete points placed on the upper chord in which the structural response signal was registered, in spite of doubling them with respect to the lower chord, the location of the defect was possible only for the transformation of the difference between signals of the undamaged and defective element. The upper chord was split into 240 elements, which gives 241 nodes. DWT demands 2^J discrete values; hence, to obtain 256 values, zeros were assumed. This results in the appearance of additional disturbances on the right side of the transformation window for some analyses (Figs. 22, 23). The damage position is precisely indicated while employing the DWT procedure and Daubechies 6 and 8 sets of wavelet functions, which is shown in Figs. 13 and 14.

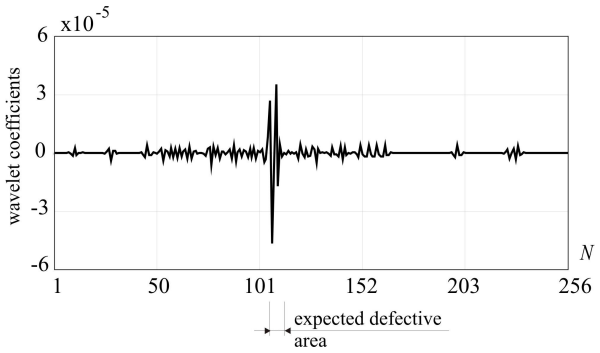

Fig. 13. 1-D DWT of vertical displacements u_z of difference between the signals of the undamaged and damaged upper chord for Daubechies 6 (detail 1) and $N = 256$ number of measurements

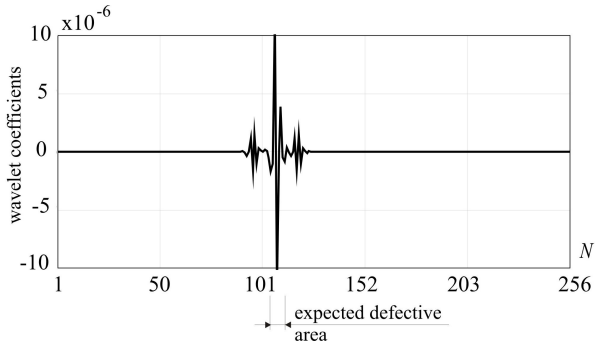

Fig. 14. 1-D DWT of angles of rotation in the plane of the girder, measured for the difference between the signals of the undamaged and damaged upper chord for Daubechies 8 (detail 1) and $N = 256$ number of measurements

4.3. Example 3. Deterioration of the diagonal – 1

The next numerical experiment is based on the analysis of damage detection occurring on selected diagonals.

The initial location of the weakened cross-section is shown in Fig. 15 in the relation to the entire single girder, whereas Fig. 16 shows the weakened cross-section in the relation to the finite

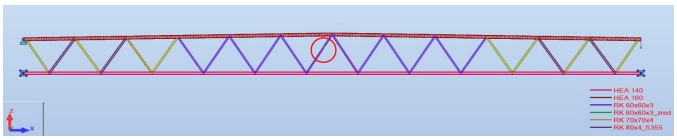

Fig. 15. Initial location of the weakened cross-section in the relation to the considered part of the whole structure

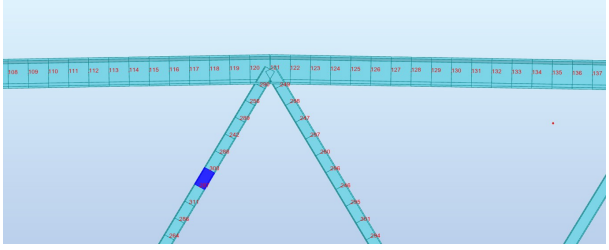

Fig. 16. Reduction of the cross-sectional stiffness in the relation to the undamaged part of the structure and finite element division

element division. The damage position is precisely indicated while employing the DWT procedure and Daubechies 6 sets of wavelet functions, which is shown in Fig. 17.

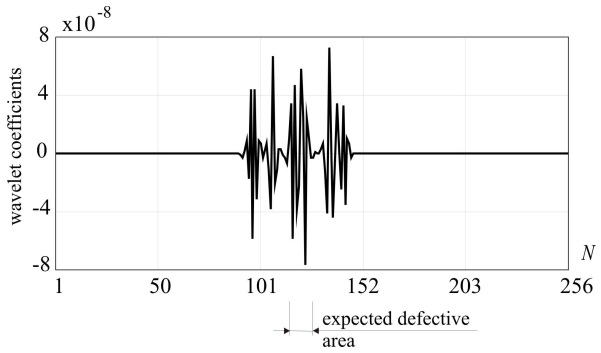

Fig. 17. 1-D DWT of angles of rotation in the plane of the girder, measured for the difference between the signals of the undamaged and damaged structure for Daubechies 6 (detail 1) and $N = 256$ number of measurements

4.4. Example 4. Deterioration of the diagonal – 2

In the following analysis two FEM elements with a reduced cross-section of diagonal were introduced (Fig. 18). The damage position is precisely indicated while employing the DWT procedure and Daubechies 4 wavelet for decomposition of the difference between the angles of rotation signals of an undamaged and a damaged girder, which is shown in Fig. 19.

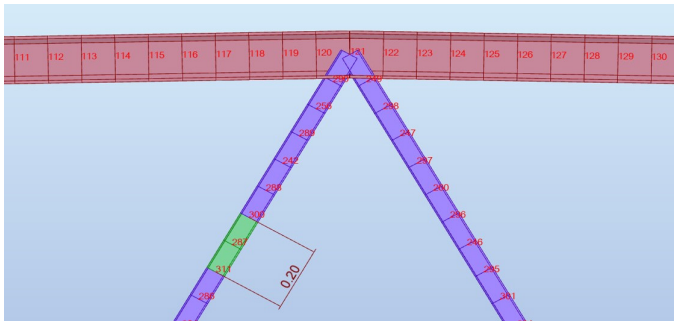

Fig. 18. Reduction of the cross-sectional stiffness in the relation to the undamaged part of the structure and finite element division

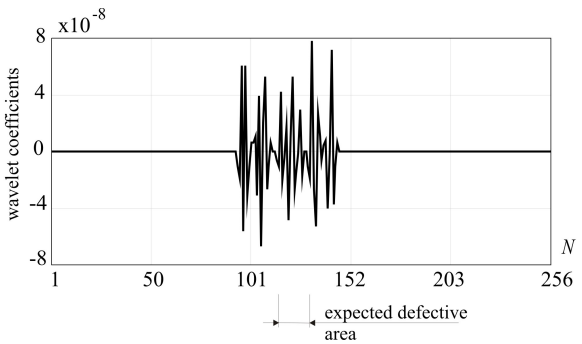

Fig. 19. 1-D DWT of the angle of rotation in the plane of the girder, measured for the difference between the signals of an undamaged and a damaged girder for Daubechies 4 (detail 1) and $N = 256$ number of measurements

4.5. Example 5. Breaking the weld

In this example, the failure of the weld was introduced. The initial location of the weakened part of a structure is shown in Fig. 20 in the relation to the entire single girder. Figure 21 presents the initial location of the damaged butt weld. The left diagonal and the upper chord are uncoupled. Breaking the connection was implemented by u_x release. The weakened part is precisely indicated while employing the DWT procedure with Daubechies 4 and 8 wavelets, which is shown in Figs. 22, 23.

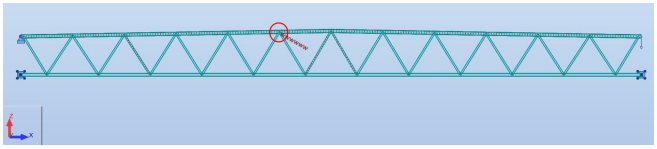

Fig. 20. Initial location of the weakened as the breaking of the weld between the upper chord and the left diagonal in the relation to the considered part of the whole structure

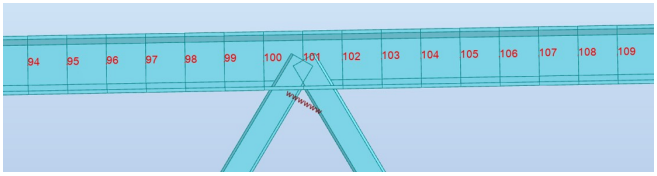

Fig. 21. Damaged butt weld at left diagonal

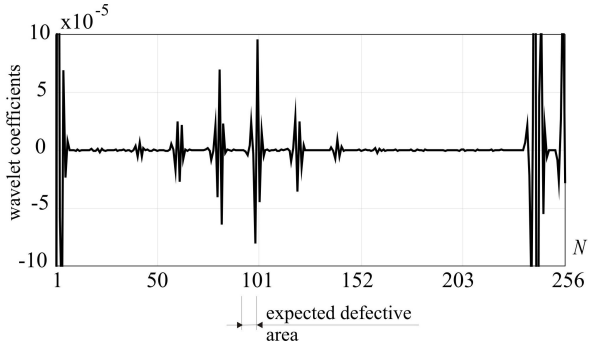

Fig. 22. 1-D DWT of vertical displacements u_z measured for the difference between the signals of the undamaged and damaged girder for Daubechies 8 (detail 1) and $N = 256$ number of measurements

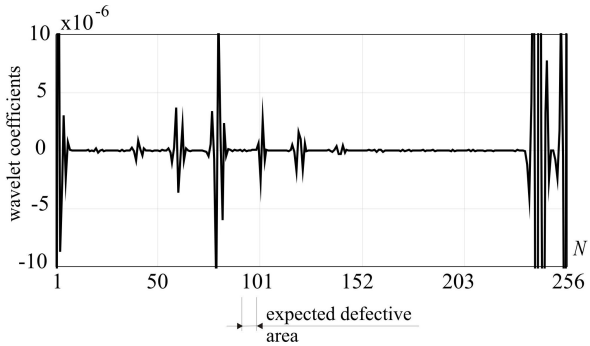

Fig. 23. 1-D DWT of angles of rotation in the plane of the girder, measured for the difference between the signals of the undamaged and damaged girder for Daubechies 8 (detail 1) and $N = 256$ number of measurements

However, the signal from the undamaged structure was necessary. In Fig. 24, the DWT of vertical displacements u_z obtained from the damaged structure reflected the location of the damage.

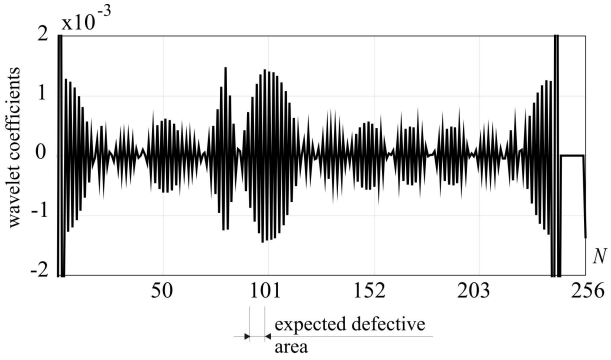

Fig. 24. 1-D DWT of vertical displacements u_z of damaged girder for Daubechies 8 (detail 1) and $N = 256$ number of measurements

4.6. Example 6. Breaking the weld – shell model

Example 5 proved that the presented approach can be used to detect damage in truss nodes. However, the signal from the undamaged structure was necessary. Herein, the shell model of a truss was used as more effective. In this scenario, it was sufficient to analyze only the response signals of a damaged girder to enhance the results.

The six-node triangular shell element with 6 DOF per node, shown in Fig. 25 is applied in the numerical investigation to obtain the structural response signal from AxisVM software.

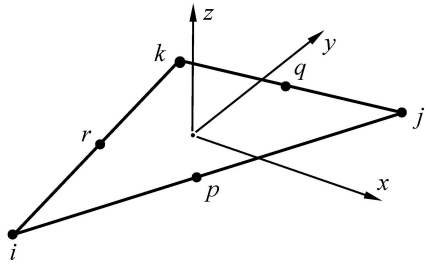

Fig. 25. Six-node triangular shell element

The flat truss girder shown in Fig. 26 is analyzed. The profiles and material properties of steel structural elements are listed in Table 7.

Table 7
Element and material properties

Element	Profile	Material	Young's modulus
Upper chord	HEA 160	S355	$210 \cdot 10^6$ [kPa]
Lower chord	HEA140	S355	$210 \cdot 10^6$ [kPa]
Diagonals	RK $60 \times 60 \times 4$	S355	$210 \cdot 10^6$ [kPa]
Columns	RK $50 \times 50 \times 3$	S355	$210 \cdot 10^6$ [kPa]

The initial location of the damaged butt weld, between the lower chord and the left diagonal, in the relation to the considered part of the whole structure is shown in Figs. 26 and 27. Weld failure was simulated by releasing the vertical displacements and angles of rotation of the nodes. The lower chord deflection line and angles of rotation, registered at discrete points (Fig. 28), as the response signals, were subjected to DWT analysis.

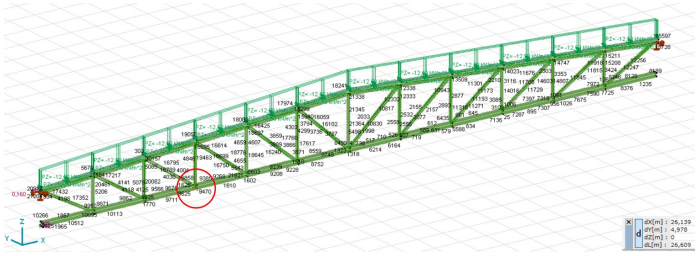

Fig. 26. Initial location of the weakened node

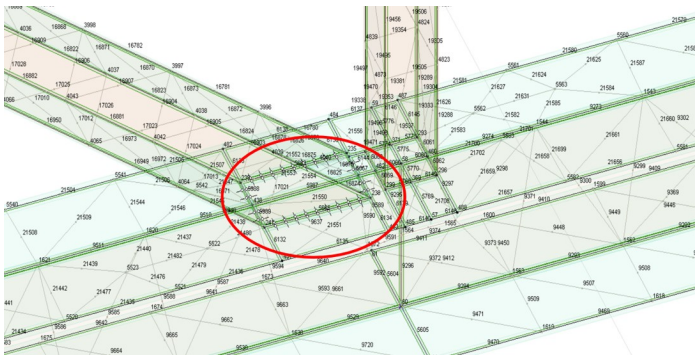

Fig. 27. Damaged butt weld at the diagonal

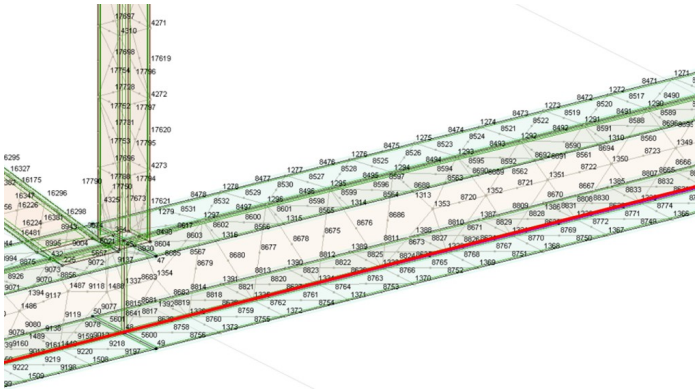

Fig. 28. Line with discrete points to record the data

The damage position is precisely indicated while employing the DWT procedure and Daubechies 6 and 8 wavelets, which is shown in Figs. 29 and 30. It is noteworthy that for DWT of vertical displacements, data recorded in only 64 points allowed the damage to be located (Fig. 29).

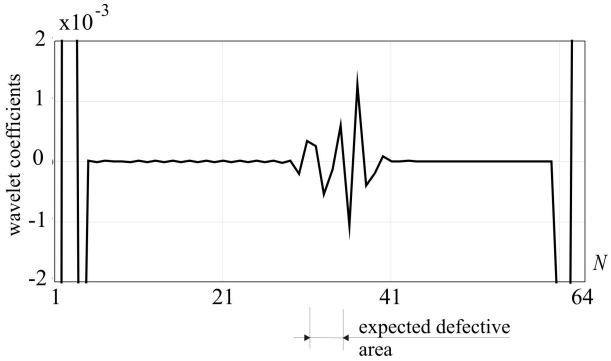

Fig. 29. DWT of vertical displacements u_z for Daubechies 6 (detail 1) and $N = 64$ number of measurement points

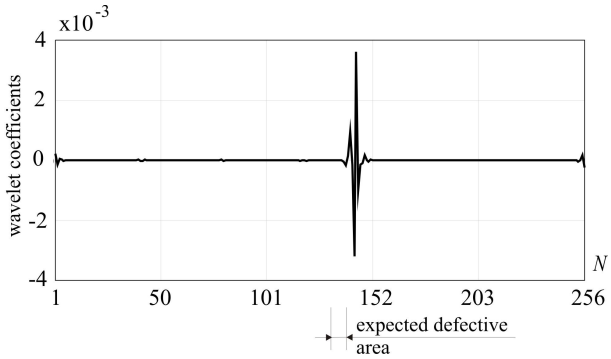

Fig. 30. DWT of angles of rotation φ_y for Daubechies 8 (detail 1) and $N = 256$ number of measurement points

5. CONCLUSIONS

In the paper, the authors present an approach to damage detection in the structural model through wavelet transformation of a discrete signal measured on a structure in the form of deflections or angles of rotation. The efficiency of the method is studied through a series of numerical examples where the real structure is simulated by a parametrized finite element model. Discrete signal decomposition using the Daubechies wavelet family of orders 4, 6 and 8 were implemented. Detail one, as the most detailed representation of the transformed signal, was taken into account. The analyses proved that the application of DWT to the decomposition of the structural response signals is very effective in determining the location of the defect. Evident disturbances of the transformed signals, including high peaks, are expected as an indicator of the defect presence in the structure. It is possible to obtain the desired information regardless of the type of defect, whether it is a stiffness reduction or a break of the welded joint. Furthermore, it should be emphasized that for the first time, the authors succeeded in the detection of a broken weld in the truss node. The efficiency of this technique is also unrelated to the number of damaged FEM elements. In the case of the lower chord deterioration location, it is sufficient to decompose the signal obtained from the damaged structure. However, in the case of the upper chord or diagonal deterioration and signal registered in discrete points located on the upper chord, for proper defect localization, the structural response of an undamaged truss structure appeared to be indispensable, despite doubling the number of measuring points. In this case, it was necessary to transform the signal difference between the damaged and undamaged structures. Nonetheless, this cannot be perceived as a disadvantage or inconvenience of the method because in the era of progressive digitization of the construction industry and construction processes called building information modeling/management (BIM) [26], it is easy to register the structural response signal after the construction, assign it to a digital asset as, e.g., a .xlsx file and treat it as a reference when monitoring the structure in subsequent years of its operation. The novel element of the research is the use of shell elements for modeling structures, which not only significantly improved the effectiveness of damage detection in the truss node but also allowed to reduce considerably the number of measurement points. In the proposed approach there is no need to build a FE model of the real structure. It is sufficient to obtain a structural response signal and subject it to DWT analysis.

ACKNOWLEDGEMENTS

Financial support by Poznan University of Technology grant 0411/SBAD/0006 is kindly acknowledged.

REFERENCES

[1] T. Kersting, *et al.* "High end inspection by filmless radiography on LSAW large diameter pipes", *NDT E Int.*, vol. 43, no. 3, pp. 206–209, 2010.

[2] P. Kołakowski, J. Szelążek, and K. Sekuła, "Structural health monitoring of a railway truss bridge using vibration-based and ultrasonic methods", *Smart Mater. Struct.*, vol. 20, no. 3, pp. 035016-1–035016-10, 2011, doi: 10.1088/0964-1726/20/3/035016.

[3] R. Drelich, M. Rosiak, and M. Pakula, "Application of non-contact ultrasonic method in air to study fiber-cement corrugated boards", *Bull. Pol. Acad. Sci. Tech. Sci.*, vol. 69, no. 2, p. e136740, 2021, doi: 10.24425/bpasts.2021.136740.

[4] R. Skłodowski, *et al.*, "Identifying subsurface detachment defects by acoustic tracing", *NDT E Int.*, vol. 56, pp. 56–64, 2013.

[5] X. Wang and J. Tang, "Structural damage detection using a magnetic impedance approach with circuitry integration", *Smart Mater. Struct.*, vol. 20, no. 3, p. 035022, 2008, doi: 10.1088/0964-1726/20/3/035022.

[6] T. Chen, *et al.* "Feature extraction and selection for defect classification of pulsed eddy current NDT", *NDT E Int.*, vol. 41, no. 6, pp. 467–476, 2008.

[7] K. Ziopaja, Z. Pozorski, and A. Garstecki, "Damage detection using thermal experiments and wavelet transformation", *Inverse Probl. Sci. Eng.*, vol. 19, no. 1, pp. 127–153, 2011.

[8] H.T. Banks and A.K. Criner, "Thermal based methods for damage detection and characterization in porous materials", *Inverse Probl.*, vol. 28, no. 6, pp. 065021-1–065021-18, 2012, doi: 10.1088/0266-5611/28/6/065021.

[9] B. Wójcik and M. Żarski, "The measurements of surface defect area with an RGB-D camera for a BIM-backed bridge inspection", *Bull. Pol. Acad. Sci. Tech. Sci.*, vol. 69, no. 3, p. e137123, 2021, doi: 10.24425/bpasts.2021.137123.

[10] D. Cekus, P. Kwiatoń, M. Šofer, and P. Šofer, "Application of heuristic methods to identification of the parameters of discrete-continuous models", *Bull. Pol. Acad. Sci. Tech. Sci.*, vol. 70, no. 1, p. e140150, 2022, doi: 10.24425/bpasts.2022.140150.

[11] T. Burczyński, W. Kuś, A. Długosz, and P. Orantek, "Optimization and defect identification using distributed evolutionary algorithms", *Eng. Appl. Artif. Intell.*, vol. 17, pp. 337–344, 2004.

[12] M. Skowron, "Application of deep learning neural networks for the diagnosis of electrical damage to the induction motor using the axial flux", *Bull. Pol. Acad. Sci. Tech. Sci.*, vol. 68, no. 5, pp. 1031–1038, 2020, doi: 10.24425/bpasts.2020.134664.

[13] Z. Waszczyszyn and L. Ziemiański, "Neural networks in mechanics of structures and materials – new results and prospects of applications", *Comput. Struct.*, vol. 79, no. 22–25, pp. 2261–2276, 2001.

[14] A. Knitter-Piątkowska, M. Guminiak, and M. Przychodzki, "Application of discrete wavelet transformation to defect detection in truss structures with rigidly connected bars", *Eng. Trans.*, vol. 64, no. 2, pp. 157–170, 2016.

[15] M. Guminiak and A. Knitter-Piątkowska, "Selected problems of damage detections in internally supported plates using one-dimensional Discrete Wavelet Transform", *J. Theor. Appl. Mech.*, vol. 56, no. 3, pp. 631–644, 2018.

[16] A. Knitter-Piątkowska and A. Dobrzycki, "Application of wavelet transform to damage identification in the steel structure elements", *Appl. Sci.*, vol. 10, no. 22, pp. 8198-1–8198-12, 2020, doi: 10.3390/app10228198.

[17] I. Daubechies, *Ten lectures on wavelets*. Philadelphia: Society for Industrial and Applied Mathematics, 1992.

[18] M. Hanteh, O. Rezaifar, and M. Gholhaki, "Selecting the appropriate wavelet function in the damage detection of precast full panel building based on experimental results and wavelet analysis", *J. Civ. Struct. Health Monit.*, vol. 11, pp. 1013–1036, 2021, doi: 10.1007/s13349-021-00497-6.

[19] M. Kamiński, "Interface defects in unidirectional composites by multiresolutional finite element analysis", *Comput. Struct.*, vol. 84, no. 19–20, pp. 1190–1199, 2006.

[20] A. Knitter-Piatkowska and T. Garbowski, "Damage detection through wavelet transform and inverse analysis," in *Proc. VI International Conference on Adaptive Modeling and Simulation ADMOS*, 2013, pp. 389–400.

[21] A. Knitter-Piątkowska and T. Garbowski, "Wavelet transform and soft computing in damage identification", in *Proc. International Conference on Engineering and Applied Sciences Optimization OPT-i*, 2014, pp. 21752188.

[22] M. Rucka and K. Wilde, "Neuro-wavelet damage detection technique in beam, plate and shell structures with experimental validation", *J. Theor. Appl. Mech.*, vol. 48, no. 3, pp. 579–604, 2010.

[23] S.G. Mallat, *A wavelet tour of signal processing*. San Diego, Academic Press, 1999.

[24] B. Svendsen, G.T. Fröseth, and A. Rönnquist, "Damage detection applied to a full-scale steel bridge using temporal moments", *Shock Vibr.*, pp. 3083752-1–3083752-16, 2020, doi: 10.1155/2020/3083752.

[25] R. Ferrari, G. Cocchetti, and E. Rizzi, "Reference structural investigation on a 19th-century arch iron bridge loyal to design-stage conditions", *Int. J. Archit. Herit.*, vol. 14, no. 10, pp. 14251455, 2020, doi: 10.1080/15583058.2019.1613453.

[26] K.M. Kensek, *Building Information Modeling*. London: Routledge, 2014.